High throughput preparation of metal oxide nanocrystals by cathodic corrosion and their use as active photocatalysts

Kromer, Matthew ; Monzo Gimenez, Francisco Javier; Lawrence, Matthew; Kolodziej, Adam; Gossage, Zachari; Simpson, Burton ; Morandi, Sara ; Yanson, Alex; Rodriguez-Lopez, Joaquin; Rodriguez, Paramaconi

DOI:
10.1021/acs.langmuir.7b02465

High throughput preparation of metal oxide nanocrystals by cathodic corrosion and their use as active photocatalysts

Matthew L. Kromer,[&#] Javier Monzo,[‡#] Matthew J. Lawrence[‡#], Adam Kolodziej,[‡#] Zachary T. Gossage,[&] Burton H. Simpson,[&] Sara Morandi,[+] Alex Yanson,[$] Joaquín Rodríguez-López,[&*] Paramaconi Rodríguez[‡*]

[&]Department of Chemistry, University of Illinois at Urbana–Champaign, Urbana, Illinois 61801, United States
[‡] School of Chemistry, University of Birmingham, Edgbaston Birmingham B15 2TT, United Kingdom
[+]Dipartimento di Chimica, Università degli Studi di Milano, via Golgi 19, 20133 Milano, Italy
[$]Cosine Measurement Systems, Oosteinde 36, 2361 HE, Leiden, The Netherlands

Abstract

Nanoparticle metal oxide photocatalysts are attractive due to their increased reactivity and ease of processing into versatile electrode formats; however, their preparation is cumbersome. We report on the rapid bulk synthesis of photocatalytic nanoparticles with homogeneous shape and size via the cathodic corrosion method, a simple electrochemical approach applied for the first time to the versatile preparation of complex metal oxides. Nanoparticles consisting of tungsten oxide (H_2WO_4) nanoplates, titanium oxide (TiO_2) nanowires, and symmetric star-shaped bismuth vanadate ($BiVO_4$) were prepared conveniently using tungsten, titanium, and vanadium wires as a starting material. Each of the particles were extremely rapid to produce, taking only 2-3 minutes to etch 2.5 mm of metal wire into a colloidal dispersion of photoactive materials. All crystalline H_2WO_4 and $BiVO_4$ particles and amorphous TiO_2 were photoelectrochemically active towards the water oxidation reaction. Additionally, the $BiVO_4$ particles showed enhanced photocurrent in the visible region towards the oxidation of a sacrificial sulfite reagent. This synthetic method provides an inexpensive alternative to conventional fabrication techniques and is potentially applicable to a wide variety of metal oxides, making the rapid fabrication of active photocatalysts with controlled crystallinity more efficient.

Introduction

Water splitting via semiconductor photocatalysts presents a promising means to store solar energy in the form of renewable fuels.[1-3] However, implementing this technology faces important challenges in materials design, engineering, and fabrication. Among the challenges for materials scientists is identifying an inexpensive material that combines excellent visible light absorption, efficient conversion, and long-term stability. The study of the impact of structural parameters on the photocatalytic performance of nano- and microparticles creates opportunities in increasing their efficiency by decreasing charge carrier diffusion lengths and therefore decreasing recombination.[4] Furthermore, the control of surface orientation, particle shape, and particle morphology enables the exploration of emerging chemical properties.[5] The use of photoactive particles also enhances the processability of large-area photoelectrodes by means of their assembly using discrete, well-defined constituent entities.

The widespread use and commercialization of semiconductor photocatalysts requires high-throughput, robust, efficient, safe, and inexpensive fabrication procedures.[6]. To date, the most common ways to prepare photocatalysts for water oxidation are solution based methods such as solvothermal syntheses[7-

[10] and electrodeposition.[11,12] In the case of solvothermal methods, time consuming synthesis procedures are usually required, and low yields are common. Such methods commonly demand the utilization of organic solvents, surfactants, or capping materials that add complexity and cost. The use of capping agents can also negatively affect the catalytic activity by blocking active sites.[13] In addition, these methods implement high temperature protocols which can result in large particle size distribution and a lack in control of the surface structure.[9] Solvothermal methods are particularly prevalent in the synthesis of various nanostructured forms of tungsten oxide and titanium dioxide. In one study, this method was employed to prepare tungstic acid hydrate nanotubes without the use of any template, [14] but the synthesis required 12 h of drying at 60°C.[14]. The solvothermal method has been used to produce TiO_2 nanosheets with preferentially oriented surfaces.[15] This synthesis required the use of hazardous precursors (TiF_4 and HF), and took 5.5-44 h to complete, with a yield of 34.8%.[15] Conversely, electrodeposition methods while offering morphological versatility,[16] suffer from low throughput. Examples of a high degree of morphological control include the use of photolithographic patterning of Cu_2O,[17] and electrodeposition of Si nanowires followed by generation of a catalyst layer.[18] In these cases, a general strategy for applying the synthesis methods to a variety of materials is lacking. A summary of recent methods for the preparation of H_2WO_4, $BiVO_4$ and TiO_2, including synthesis time, advantages and disadvantages is shown in the Supporting Information Table S1. These examples underscore the opportunity for developing methods capable of creating complex photocatalytic materials with high throughput and in a timely manner.

Here we report the utilization of the cathodic corrosion method[19,20] for the preparation of metal oxide and mixed metal oxide photocatalysts. This method has shown the potential to prepare metal and metal alloy nanoparticles with high morphological homogeneity and well-defined composition.[19-21] Additionally, it has the capability to modulate particle size and shape by means of versatile adjustments of the potential waveform applied to the electrode. An early report demonstrated that the cathodic corrosion method can be used in the preparation of TiO_2 nanoparticles. However, these nanomaterials were used as support for Au nanocatalyst and not directly as a photoactive material.[22] Since the method does not require the utilization of organic solvents, surfactants, or capping ligands, metal nanocatalysts produced through this method have shown extraordinary catalytic activity.[21] In this report, we take a step forward and demonstrate the utility of cathodic corrosion as a synthetic method to prepare complex oxide nanoparticles of H_2WO_4, TiO_2, and $BiVO_4$ with unprecedented simplicity and particle size homogeneity. All of the syntheses were done on the order of minutes, making this method far superior in terms of time to any of the more commonly used synthetic methods for preparing nanoparticulate

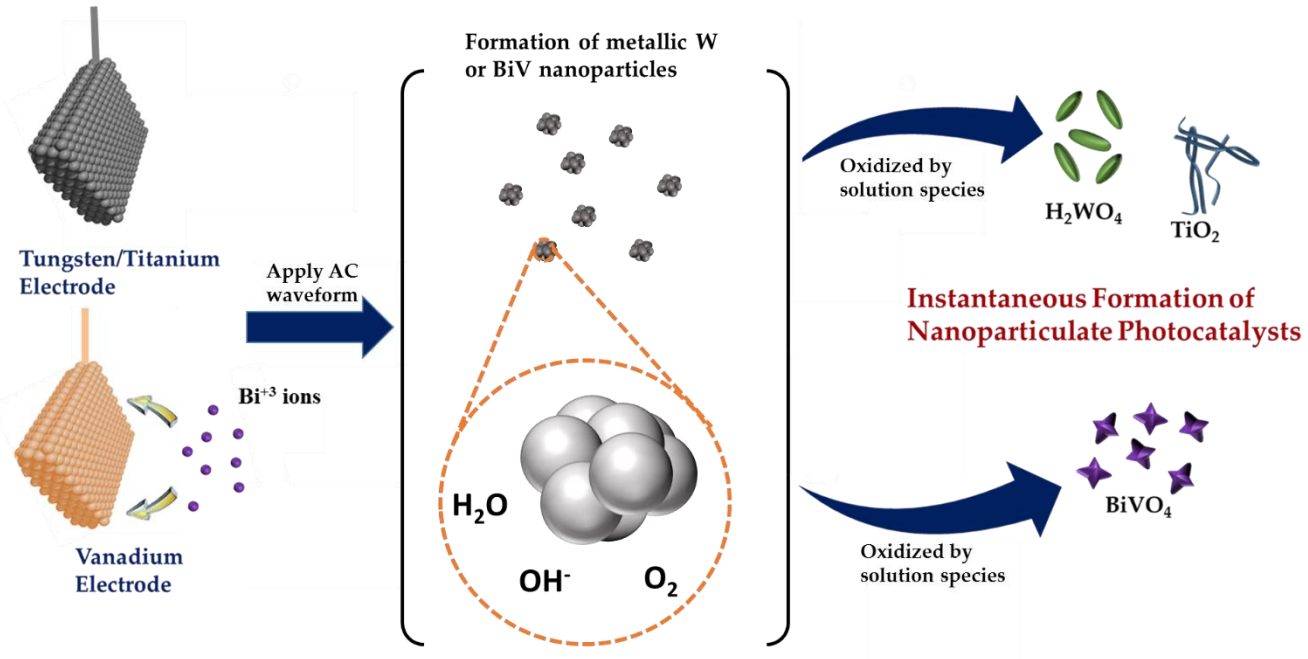

Figure 1: Schematic depicting how cathodic corrosion was used to prepare H_2WO_4, TiO_2, and $BiVO_4$ photocatalysts.

photocatalysts. In addition, the control achieved over the crystallinity of the H_2WO_4 and $BiVO_4$ nanoparticles is indicative that such control could be also achieved on other metal oxides by changing electronic parameters such as amplitude or frequency of the AC wave, or by changing chemical parameters such as concentration or nature of the cation.

Experimental

Synthesis and Characterization of Particles

The method by which these particles were synthesized is summarized in Figure 1. For the synthesis of H_2WO_4 particles, 2.5 mm of a tungsten wire (diameter of 0.127 mm, Rembar Co. LLC, USA) was submerged in a 1 M solution of $KHSO_4$. A square wave voltage in the range of 0 V to -10 V was applied between a W wire (working electrode) and a high surface area Pt foil (counter electrode) resulting in the instantaneous formation of the nanoparticles. The TiO_2 nanowires were prepared with a 0.2 mm diameter titanium wire that was subjected to an AC square wave in the range of 0 V to -10 V with a frequency of 100 Hz while immersed in a 10 M NaOH solution. The $BiVO_4$ nanoparticles were synthesized using a vanadium wire with diameter of 0.15 mm (99.8 % Alfa Aesar). This wire was immersed in 10 mL of a mixture (1:1 by volume) of saturated $CaCl_2$ solution and MilliQ water (Elga, 18.2 MΩ cm, 1 ppb total organic carbon), in which 750 µL of a saturated Bi_2O_3 solution was subsequently added. The synthesis was successfully achieved by applying a square wave voltage in a range of -8 V to 2 V. In each of the syntheses, current and time was monitored using a National Instruments DAQ module (NI-6211). Once synthesized, the resulting suspensions of nanoparticles were centrifuged at 3000 rpm for 20 minutes and suspended in ElgaPure water to remove the excess electrolyte. UV-vis spectroscopy was employed to elucidate species present in $KHSO_4$ solution immediately after cathodic corrosion of W wire and in the resultant supernatant solution after centrifugation at 4000 RPM for 3 minutes, using a Varian Cary 50 UV-Vis Spectrophotometer.

The crystal structures of the prepared particles were determined using a BRUKER D2 Phaser powder X-ray diffractometer operating at 30 kV, 10 mA and a Co-Kα (0.179 nm) radiation source. The X-ray diffraction (XRD) data are reported on a 2θ angle scale of a Co-Kα radiation source for an appropriate comparison with values from the JCPDS database. The samples were prepared by depositing 25 µL of the aqueous nanoparticle suspensions on a zero background SiO (MTI) holder and dried under air atmosphere.

The particle size distribution and shape of the particles were determined by transmission electron microscopy (TEM) using a JEOL JEM 1200 EX MKI instrument and the particle thickness was determined by contact mode atomic force microscopy (AFM), obtained under ambient pressure and temperature conditions, using an AFM microscope Veeco metrology, equipped with a NanoScope IIIa controller and using a 200 µm cantilever with a pyramidal silicon nitride tip (spring constant 0.12 Nm^{-2}). Compositional analysis was determined by X-ray fluorescence (XRF) using a Bruker S8 Tiger 4 kW spectrometer under a helium atmosphere. The particle morphology and composition was confirmed by scanning electron microscopy (SEM) in a JEOL 2100 Scanning electron microscope instrument coupled with energy dispersive X-ray spectroscopy (EDX).

Photoelectrochemical Measurements

In order to study the photoactivity of the particles, they were first integrated into a photoelectrode. The suspended particles were drop cast in volumes of 20 µL onto an indium tin oxide (ITO) cover slip (SPI Instruments 15-30 Ω). Next, 100 µL of 5 wt% Nafion® perfluorinated resin solution (Sigma Aldrich) were spun-cast onto the particles at 1200 rpm for 3 minutes to prevent the particles from detaching from the ITO when immersed in solution. Electrical connection was made to the ITO slide by using copper tape (3M Electrical Products). In the case of $BiVO_4$, particles were drop cast as 3 layers of 20 µL to

increase the overall particle concentration on the surface of the ITO cover slip. The photoelectrochemical measurements were carried out in a custom made 3 mL Teflon cell and the potential of the photoelectrodes was controlled via either CHI760E or 920D workstations (CHI Instruments) in a three-electrode setup. The reference electrode used was a Ag/AgCl (3M KCl) with a $NaClO_4$ agar salt bridge and all potentials reported are versus Ag/AgCl unless otherwise stated. The counter electrode was 1 mm diameter Pt wire. All measurements were performed in 0.1 M NaOH under illumination from a 6258 Oriel Xe lamp. Incident photon-to-electron conversion efficiency (IPCE) spectra were taken by filtering this source using a Newport Oriel 1/8m Cornerstone monochromator.

Results and Discussion

The reaction mechanism of the cathodic corrosion method for the formation of the nanoparticles proceeds via the formation of the metal anion stabilized by the cations, other rather than protons, present in the solution. In order to confirm this reaction mechanism in the formation of the tungsten nanoparticles via cathodic corrosion, a tungsten wire was immersed in a solution of 0.1 M H_2SO_4 and a AC wave form between 0 and -10 V with a frequency of 100 Hz was applied during 120 s. Under these conditions, only hydrogen evolution was observed (see video S1 in supporting information). In contrast, when the same AC wave form conditions were applied in a solution containing 1 M $KHSO_4$, the reaction resulted in an aqueous nanoparticle dispersion (see video S2 in supporting information). Given that the electrochemical conditions are identical and the pH in both solutions is similar, we conclude that the presence of the metal cation is requisite for the formation of the nanoparticles and therefore the cathodic corrosion is the dominant reaction mechanism. Furthermore, we propose that the formation of tungsten metallic nanoparticles proceed via the formation of an anion intermediate stabilized by the cation in solution and the oxidation of this intermediates to tungsten nanoparticles. The tungsten

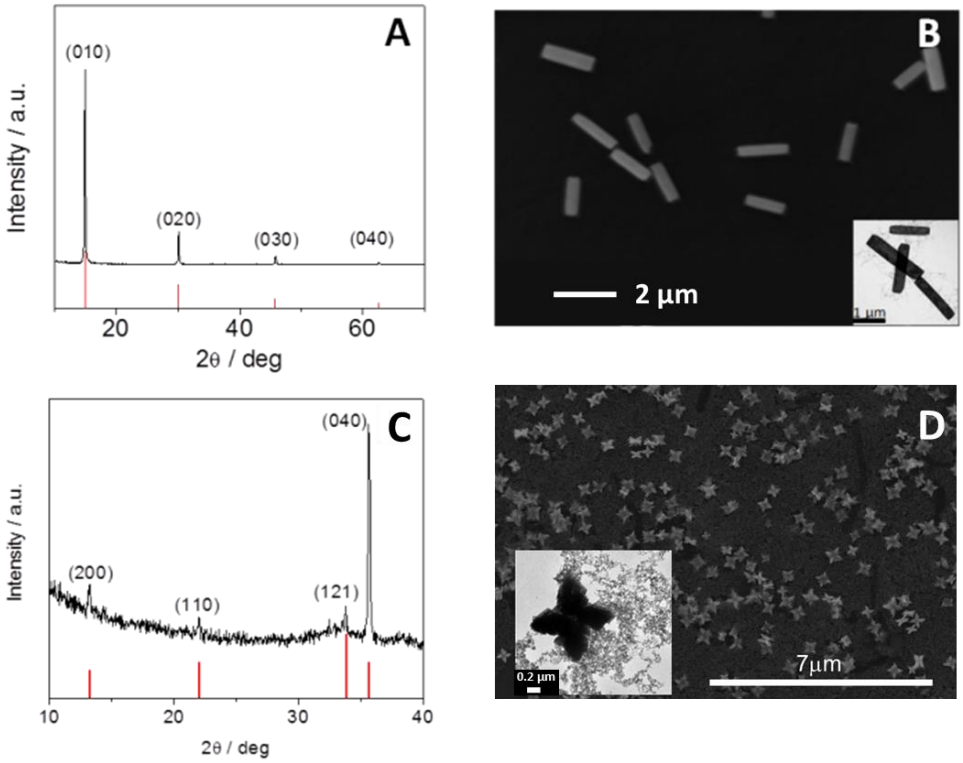

Figure 2: X-ray diffraction patterns and SEM images of (A, B) H_2WO_4 and (C, D) $BiVO_4$. The insets on the SEM images correspond to the HR-TEM images of the nanoparticles.

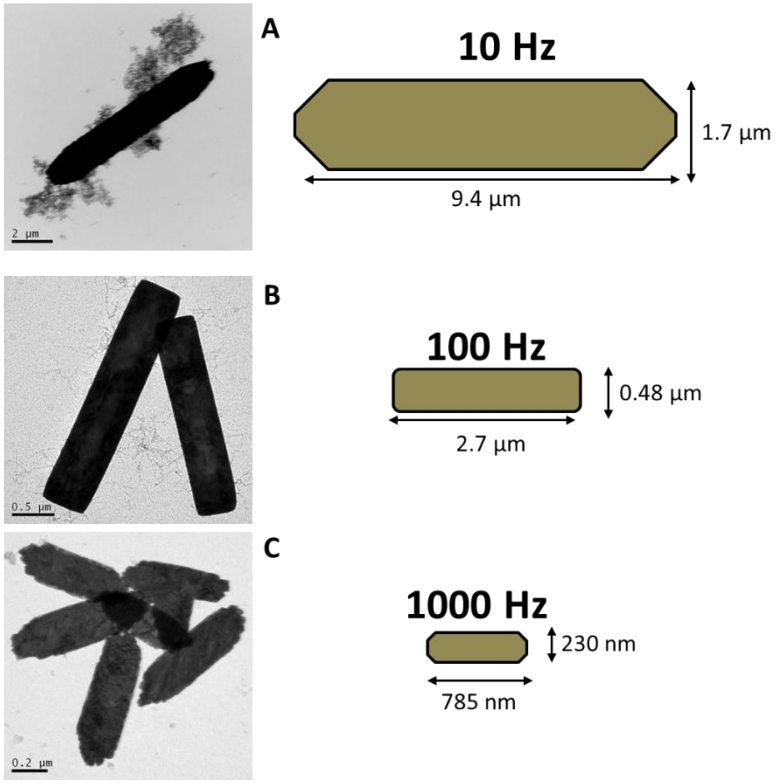

Figure 3: TEM images and schematic of the H_2WO_4 particles prepared by cathodic corrosion in a 1 M solution of $KHSO_4$ with a square wave voltage between 0 V to -10 V and different frequencies (A) 10 Hz, (B) 100 Hz and (C) 1000 Hz.

nanoparticles are prompt to oxidation in water,[23] resulting in the formation of WO_2 and subsequently to WO_3 and H_2WO_4.[24 2] In a similar fashion, previous work has shown the synthesis of SnO_2 nanoparticles via two-step process involving the cathodic corrosion.[25] We propose that the formation of $BiVO_4$ nanoparticles proceed via the formation of a multimetallic anion intermediate $(BiV)^{-n}$ on the surface of the vanadium upon the reduction of the Bi^{+3} similar to the reaction mechanism proposed for the formation of PtBi nanoparticles.[21] However, we do not discard the possibility that the positive potential applied during the square wave program influence in the reaction mechanism and geometry of the nanoparticles.

We analysed a freshly-prepared solution and its supernatant via UV-Vis in order to discard the presence of ionic W species. As can be seen in Figure S1, the spectra of the freshly prepared solution shows one broad adsorption band between 200 nm and 400 nm, associated to the presence of WO_2/WO_3 colloidal nanoparticles. After the nanoparticles were centrifuged, the supernatant did not show any adsorption band. Therefore, the presence of dissolved cationic tungsten species was discarded.

Morphological Characterization

After the synthesis of the nanoparticles of H_2WO_4 and $BiVO_4$ by cathodic corrosion, their crystal structure, composition, and particle size were studied by XRD, SEM/EDX, and TEM as shown in Figure 2, and by XRF as shown in Figure S4. XRD patterns for representative H_2WO_4 particles obtained at a frequency of 100 Hz are shown in Figure 2A. The 2θ angle at 14.8 indicates a preferential orientation along the (010) plane (JCPDS no. 18-1420). In the case of H_2WO_4, a colloidal suspension

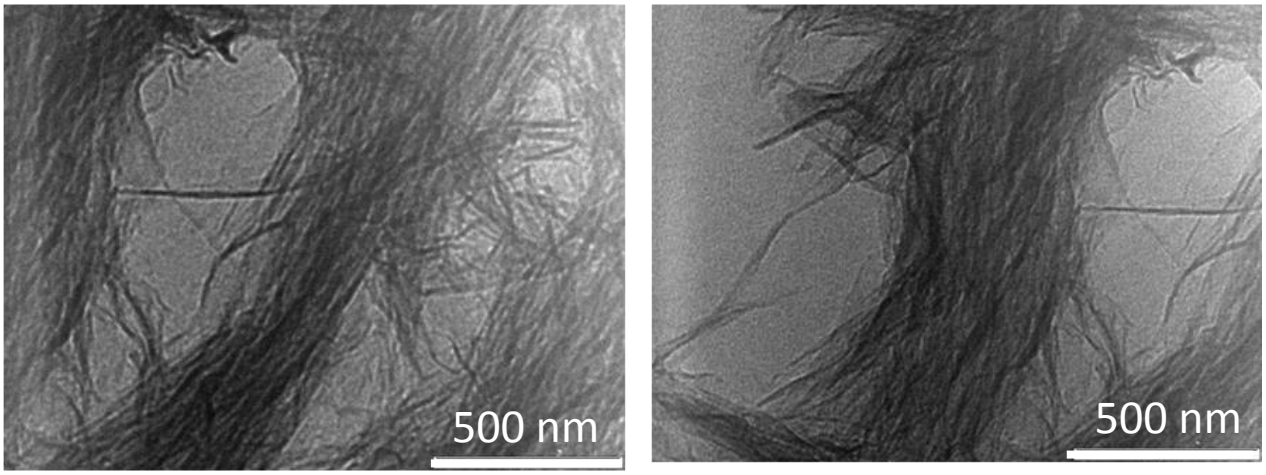

Figure 4: TEM of TiO_2 nanoparticles prepared by cathodic corrosion from a Ti wire in a 10 M NaOH solution using an AC square wave between -10 and 0 V with 100Hz frequency.

was always observed after cathodic corrosion, although the XRD pattern exhibited an evolution in time, as shown in Figure S2. The SEM/TEM images of the H_2WO_4 shows presence of H_2WO_4 nanorods/nanoplates with homogenous size and consistent shape (Figure 2B). The particle size distribution (Figure S5) was found to be 2.7 ± 0.2 µm in length and 0.5 ± 0.1 µm in width. In addition to the particle size obtained by TEM and SEM measurement, the AFM measurements (Figure S6) have shown that the H_2WO_4 nanoparticles have 61±10 nm height. One of the most interesting aspects that we found for the cathodic corrosion synthesis of H_2WO_4 was its versatility for controlling the size and shape of the particles. Even though, the control on the size and shape has been probed for the synthesis of platinum nanoparticles,[26,27] the control of the size and shape of metal oxides open a new dimension of application of these materials. Until now, such control was limited by the application of high temperatures during the synthesis protocol and due to harsh conditions used to clean the capping materials and surfactants. As shown in Figure 3, the shape and size of the nanoparticles was tuned by simply changing the frequency of the square wave voltage. Choosing this external input allows us to change the size of the H_2WO_4 by an order of magnitude from hundreds of nanometers to few microns (Figure 3).

Figure 2C shows the X-ray pattern of the $BiVO_4$ nanoparticles which indicates the presence of (040) preferential orientation (JCPDS no. 14-0688). The SEM/TEM images show star-like shape nanoparticles with homogenous size of 1.1 ± 0.1 µm. The AFM cross section of the $BiVO_4$ nanoparticles (Figure S6) shows that the particles are 35±12 nm height. The composition of the $BiVO_4$ nanoparticles was confirmed by XRF and EDX analysis (Figure S4). Synthesis of $BiVO_4$ has demonstrated the capabilities of the cathodic corrosion method to prepare complex oxides by the addition of solution-phase components in the synthesis media. Future work will contemplate the control of the particle size, shape and composition as a function of chemical and electrochemical parameters such as amplitude and cation concentration. Although it is difficult to estimate the Faradaic yield for any of the samples

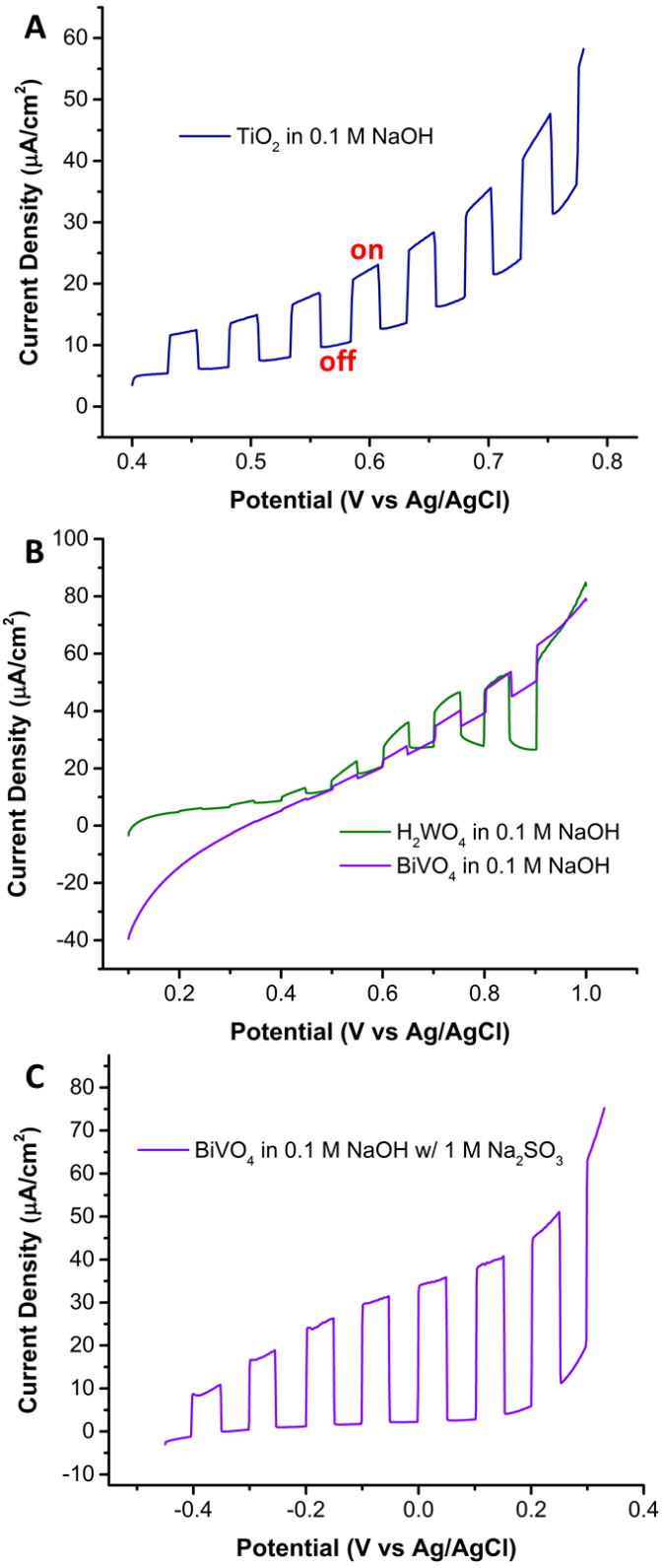

Figure 5: Chopped light linear sweep voltammograms of the nanoparticulate photocatalysts prepared through cathodic corrosion. A) Linear sweep voltammogram for TiO_2 in 0.1 M NaOH. B) Linear sweep voltammogram for the 100 Hz H_2WO_4 and $BiVO_4$ particles in 0.1 M NaOH. C) The same experiment shown in A repeated for $BiVO_4$ in 1 M Na_2SO_3.

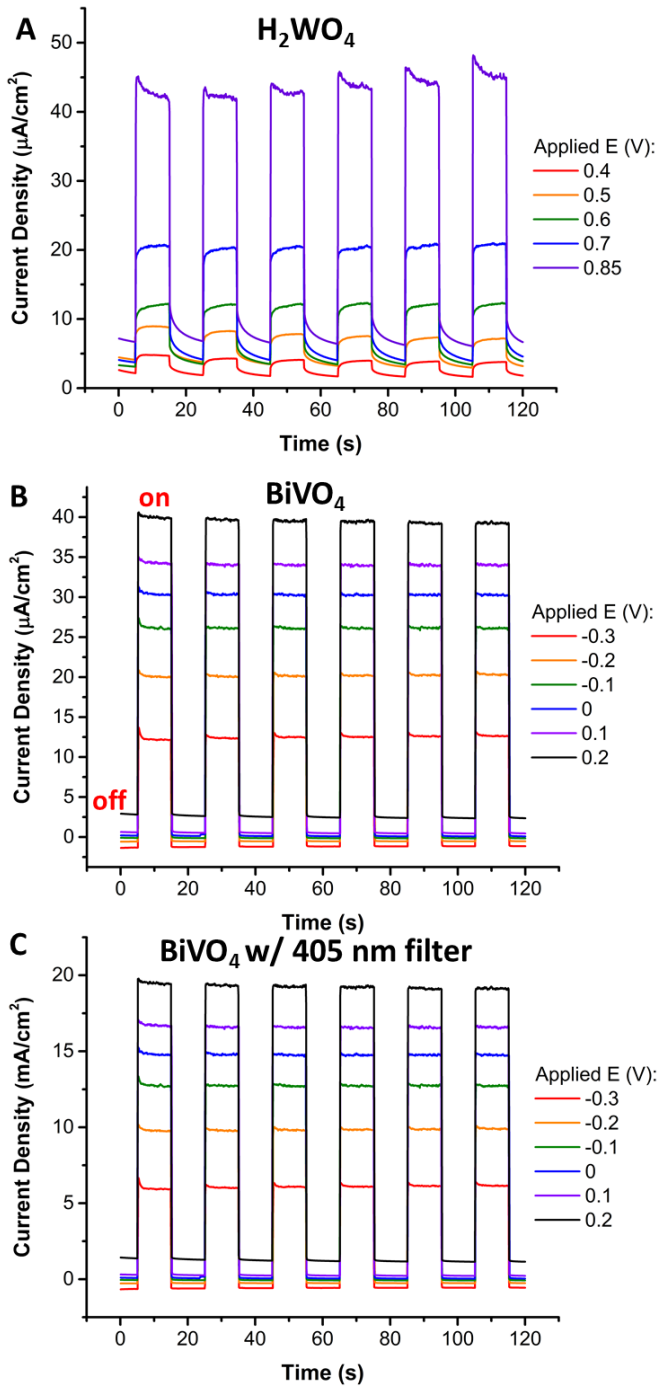

Figure 6: Photocurrent as a function of potential for the H_2WO_4 (A) and $BiVO_4$ (B) particles, respectively, prepared via cathodic corrosion. The chronoamperometry in (C) is the same $BiVO_4$ particles being illuminated with only visible light. Measurements were taken in 1 M Na_2SO_3 for $BiVO_4$ and 0.1 M NaOH for H_2WO_4 and both were illuminated with 60 mW/cm^2 for the chronoamperometry experiments.

prepared, the obtained powders exhibited only slight amounts of the V_2O_5 phase, displaying largely the correct crystal structure for $BiVO_4$.[28,29] Finally, the characterization by TEM of the TiO_2 nanoparticles is presented in Figure 4. The size of the TiO_2 nanowires was approximately 500-800 nm in length and 4-8 nm in diameter. Despite the morphological conservation among the TiO_2 nanowires, there was no periodic crystal structure which resulted in the absence of any XRD pattern.

Under the conditions presented here the rate of formation of particles was the highest for the H_2WO_4, taking approximately 60-100 s to etch 2.5 mm of wire (Figure S7). The $BiVO_4$ took a similar time of 100-160 s to etch 2.5 mm of wire, and the TiO_2 took a longer time of 250-320 s to also etch the same amount of wire. The nanoparticles are collected by centrifugation as described in the experimental section after etching 5-7.5 mm of the wires and we observed that quantities on the order of milligrams could be produced from all samples. Yields of 38±9 %, 61±7 % and 66±10 % have been achieved for H_2WO_4, $BiVO_4$ and TiO_2. Losses in mass of the nanoparticles take place during the synthesis process by attachment of the nanoparticles to the counter electrode and during the process of centrifugation and removal of the excess of electrolyte. It has been also observed that TiO_2 nanoparticles lack in stability in the NaOH solution, therefore a quick washing procedure is required to avoid major losses due to dissolution of the TiO_2 nanoparticles.

Because of the different synthesis conditions and varying sizes of the metal wires, it is difficult to draw comparisons between each of the nanoparticles. Despite the successful preparation of oxide particles from various parent metals, there are several aspects yet to be understood about the cathodic corrosion method applied to these samples, including the etching time and its relationship with the resulting particle size and crystallinity of the sample. We propose that the changes in size and shape are influenced by the concentration of intermediate species (anionic and/or metallic) in solution. This intermediate species concentration is modified by changes in the frequency and amplitude of the applied waveform, as well as by the stabilizing cation concentration in solution (here, K^+). Similar changes in size and shape were also observed during the formation of Pt, Au and Rh nanoparticles as a function of these factors.[26,27,30] Furthermore, it is plausible that the kinetics of

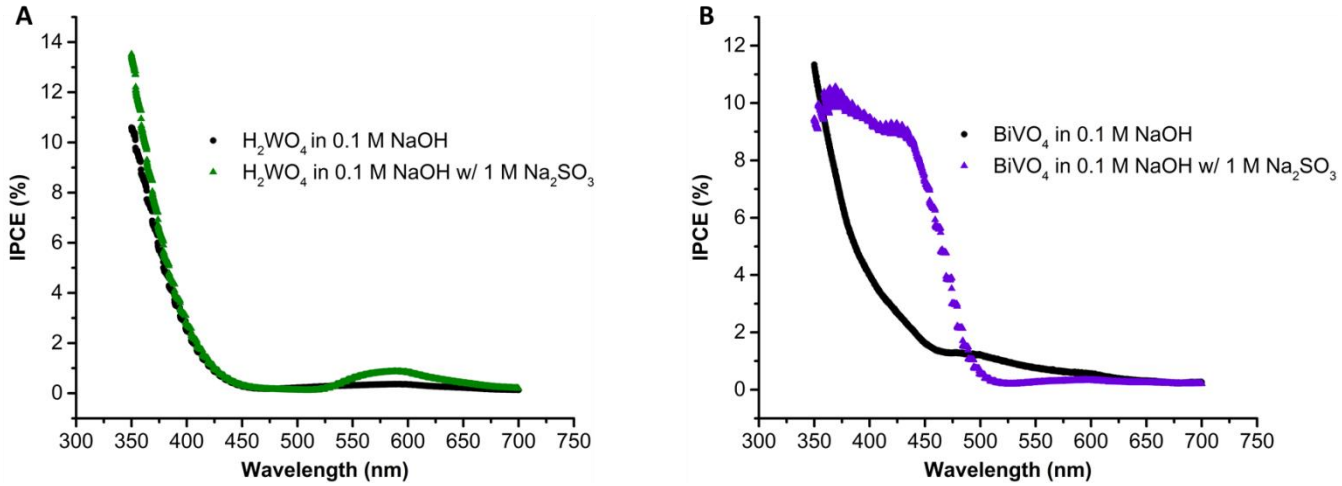

Figure 7: IPCE spectra for the H_2WO_4 (A) and $BiVO_4$ (B) particles depicting an appropriate band edge for each. Measurements were taken in 0.1 M NaOH with and without 1 M Na_2SO_3.

nanoparticle oxidation ($W \rightarrow WO_x$) will be affected by the size of the particles generated after cathodic corrosion.[23] In addition, other factors such as changes in zeta potential may occur. Therefore, we postulate that differences in nanoparticle shape and size are induced by chemical processes that take place after the electrochemical etching step, but that nonetheless are a product of the chosen cathodic corrosion parameters.

Other than the frequency of the waveform, we are currently investigating other parameters that govern the etching time, size, shape, and composition of the particles. Currently our groups are studying the effect of electrolyte composition and potential thresholds during cathodic corrosion on particle size and shape and this will be subject of a forthcoming publication.

Electrochemical Characterization

We now turn to evaluate the photoelectrochemical reactivity of the obtained particles. Chopped light linear sweep voltammetry was used to determine the relative activation of the particles towards water oxidation and is shown in Figures 5A and 5B. Due to the relatively low surface coverage and the Nafion® partially covering some of the particles, the photocurrent density scale is fairly low for the H_2WO_4/ITO, $BiVO_4$/ITO, and TiO_2/ITO electrodes. However, as a reference point unsintered semiconductor particle films yield photocurrents on the order of μA cm^{-2}.[31] The H_2WO_4 and TiO_2 particles, prepared with a square wave function at 100 Hz, yielded photocurrent values on the same order of magnitude, and the $BiVO_4$ resulted in the lowest activity. The photocurrent shown by TiO_2 nanowires, despite having no defined crystal structure, is strongly suggestive of a mixture of photoactive crystal domains. As stated earlier, the crystallinity of nanoparticles may be dependent on the rate of corrosion, and if so, then we hypothesize that highly crystalline TiO_2 photocatalysts can also be prepared. Despite the higher crystallinity of the obtained samples for $BiVO_4$, its low activity toward water oxidation has been well-documented,[32,33] where the addition of Na_2SO_3 acting as a hole scavenger improved the current magnitude significantly. As shown in Figure 5C, the presence of Na_2SO_3 increased the photocurrent of $BiVO_4$ to be comparable to the H_2WO_4 nanoparticles and TiO_2 nanowires. This demonstrates that these photocatalysts all possess relatively similar activity so long as they are carrying out a kinetically facile reaction – sulfite oxidation in the case of $BiVO_4$. We have successfully demonstrated the preparation of photoactive $BiVO_4$ particles through cathodic corrosion, but the challenge remains to fabricate $BiVO_4$ that is highly active toward water splitting. This will most likely be enabled through the inclusion of dopants in solution during the synthesis that are known to enhance the adsorption and interfacial charge transfer kinetics between $BiVO_4$ and H_2O to form O_2.[34,35]

Chronoamperometry of H_2WO_4 and $BiVO_4$ nanoparticles was utilized to investigate the presence of transient processes upon illumination. In the case of H_2WO_4, there is an initial decrease in current under illumination at high activation (Figure 6A). This decrease in current is likely due to charge recombination in the H_2WO_4 particles. This current transient is not observed for $BiVO_4$, and is likely due to the size difference between the particles. The H_2WO_4 particles are larger than the $BiVO_4$, which results in longer distances for holes to reach the surface. Since the $BiVO_4$ particles are much smaller than the H_2WO_4 particles, there is no observable charge recombination occurring. While seemingly detrimental to photocatalyst performance, this recombination is not too concerning since it only occurred at large applied biases.

We tested the spectral response of the obtained particles. Figure 6C shows the chopped chronoamperometry with the $BiVO_4$ particles under illumination through a 405 nm cutoff filter. We observed that the $BiVO_4$ retained about half of the current density when only illuminated with visible light. Chopped chronoamperometry under visible light was also collected for the H_2WO_4 particles, but large activity was not observed (Figure S9) due to the relatively small amount of visible light that H_2WO_4 can be expected to absorb. We hypothesize that cathodic corrosion could also be used to incorporate dopants for increasing the visible light response of the resulting nanoparticles. Certain dopants have already been shown in the literature to red shift the band edge of WO_3,[36-38] and could bolster the visible activity of H_2WO_4 particles.

Because crystalline $BiVO_4$ and H_2WO_4 particles absorb some portion of visible light, an IPCE spectrum was obtained for each to determine the wavelength cutoff of their band edges (Figure 7). A spectrum was acquired for each in the presence and absence of Na_2SO_3, which acted as a hole scavenger. The IPCE spectra for the H_2WO_4/ITO shows a cutoff around 440 nm, which is similar to what is expected for an electrodeposited film of H_2WO_4.[12,39] It also shows very slight differences in the presence of a hole scavenger, thus suggesting that interfacial charge transfer is not limiting in these particles. Additionally, the IPCE for H_2WO_4 shows a marked increase from 550 nm to 650 nm, which may be due to the presence of defects in the crystal structure.

These defects reside at an energy in between the conduction and valence band, which results in electrons occupying these states to be excited by longer wavelengths of light.[40,41] In the absence of a hole scavenger, a poor IPCE spectrum was obtained for $BiVO_4$, which is due to very slow reaction kinetics to carry out water oxidation. In contrast, upon addition of Na_2SO_3, the IPCE for the $BiVO_4$ particles showed a band edge around 510 nm, which corresponds well with what has been reported in the literature.[28,29] Altogether these measurements confirm the ability of the cathodic corrosion method to yield photoactive metal oxides with unique morphologies using a simple synthetic approach.

Conclusion

We show for the first time the application of cathodic corrosion to produce metal oxides and mixed metal oxide nanoparticles with an outstanding homogeneity of particle size and shape. All of the particles studied here were made on the order of minutes, which greatly improves upon standard photocatalyst nanoparticle synthesis procedures. Amorphous TiO_2, and crystalline H_2WO_4 and $BiVO_4$ nanoparticles were prepared with preferential crystallographic orientation starting from the base metal as the reactant. In all cases, we observed the successful incorporation of oxygen the lattice as confirmed via XRD and EDX. We also illustrated for H_2WO_4 that the frequency of the excitation waveform can greatly impact the particle size. The cathodic corrosion method can be very easily modified to produce particles with a variety of sizes. In addition, the successful preparation of $BiVO_4$ underscores the exciting possibilities for the synthesis of multi-metallic oxides and the incorporation of dopants using simple solution precursors. Although the TiO_2 did not possess a high degree of crystallinity, it was nonetheless photoactive toward water oxidation. The H_2WO_4 and $BiVO_4$ both were crystalline, and

H_2WO_4 carried out water oxidation under illumination. The $BiVO_4$ prepared with cathodic corrosion was not able to appreciably carry out water splitting, but displayed facile conversion of sulfite under both UV-vis and visible only illumination. This ability for $BiVO_4$ to effectively facilitate photochemical oxidation of sulfite under only visible light was displayed through chopped light chronoamperometry and the obtained IPCE spectrum. Future work will investigate alternatives to adhering particles to a surface that do not alter morphology or crystal orientation.[42,43]

We demonstrated the potential of the cathodic corrosion method for the straightforward synthesis of particles with well-defined morphology and composition. This creates opportunity in the low-cost production of large quantities of processable particles that can streamline the preparation of efficient electrodes for photocatalysis. The cathodic corrosion method is prompt for industrial scale up: the method avoids large volumes of organic solvents and the ensuing large investments in heating and cleaning treatment and safety and disposal issues. Finally, the time of synthesis of the catalyst is an important parameter to consider for further industrial applications. While other methods might require several hours or days of preparations, we have shown the time-effectiveness of the method to prepare particles in minutes. There is still much work to be done toward the effect that various parameters such as etching time or solution composition have on the resulting particles. Despite this, cathodic corrosion was shown here to be a facile alternative method for producing metal oxide nanoparticles.

AUTHOR INFORMATION

Corresponding Authors

*joaquinr@illinois.edu
*p.b.rodriguez@bham.ac.uk

Author Contributions

#These authors contributed equally.

ACKNOWLEDGMENT

We acknowledge support from the Transatlantic Collaboration Fund and the BRIDGE program between the University of Illinois and the University of Birmingham. PR would like to acknowledge the University of Birmingham for the financial support through the Birmingham fellowship program. JM,MJL and AK acknowledge the University of Birmingham for the financial support through PhD scholarships at the School of Chemistry.

REFERENCES

(1) Gratzel, M. Photoelectrochemical cells. *Nature* **2001**, *414*, 338-344.
(2) Bolton, J. R. Solar photoproduction of hydrogen: A review. *Sol. Energ.* **1996**, *57*, 37-50.
(3) Gust, D.; Moore, T. A.; Moore, A. L. Solar Fuels via Artificial Photosynthesis. *Acc. Chem. Res.* **2009**, *42*, 1890-1898.
(4) Memming, R. Photoinduced Charge-Transfer Processes at Semiconductor Electrodes and Particles. *Electron Transfer I* **1994**, *169*, 105-181.
(5) Li, D.; Haneda, H. Morphologies of zinc oxide particles and their effects on photocatalysis. *Chemosphere* **2003**, *51*, 129-137.
(6) Lewis, N. S. Research opportunities to advance solar energy utilization. *Science* **2016**, *351*, 1920.
(7) Choi, H. G.; Jung, Y. H.; Kim, D. K. Solvothermal synthesis of tungsten oxide nanorod/nanowire/nanosheet. *J. Am. Ceram. Soc.* **2005**, *88*, 1684-1686.
(8) Jiao, Z. H.; Wang, J. M.; Ke, L.; Sun, X. W.; Demir, H. V. Morphology-Tailored Synthesis of Tungsten Trioxide (Hydrate) Thin Films and Their Photocatalytic Properties. *ACS Appl. Mater. Interfaces* **2011**, *3*, 229-236.
(9) Waller, M. R.; Townsend, T. K.; Zhao, J.; Sabio, E. M.; Chamousis, R. L.; Browning, N. D.; Osterloh, F. E. Single-Crystal Tungsten Oxide Nanosheets: Photochemical Water Oxidation in the Quantum Confinement Regime. *Chem. Mater.* **2012**, *24*, 698-704.
(10) Lee, K.; Seo, W. S.; Park, J. T. Synthesis and optical properties of colloidal tungsten oxide nanorods. *J. Am. Chem. Soc.* **2003**, *125*, 3408-3409.
(11) Baeck, S. H.; Jaramillo, T.; Stucky, G. D.; McFarland, E. W. Controlled electrodeposition of nanoparticulate tungsten oxide. *Nano Lett.* **2002**, *2*, 831-834.

(12) Su, L. Y.; Zhang, L. G.; Fang, J. H.; Xu, M. H.; Lu, Z. H. Electrochromic and photoelectrochemical behavior of electrodeposited tungsten trioxide films. *Sol. Energ. Mat. Sol. Cells* **1999**, *58*, 133-140.
(13) Kim, C.; Lee, H. Change in the catalytic reactivity of Pt nanocubes in the presence of different surface-capping agents. *Catalysis Communications* **2009**, *10*, 1305-1309.
(14) Zhao, Z. G.; Miyauchi, M. Nanoporous-walled tungsten oxide nanotubes as highly active visible-light-driven photocatalysts. *Angew. Chem. Int. Ed.* **2008**, *47*, 7051-7055.
(15) Yang, H. G.; Liu, G.; Qiao, S. Z.; Sun, C. H.; Jin, Y. G.; Smith, S. C.; Zou, J.; Cheng, H. M.; Lu, G. Q. Solvothermal Synthesis and Photoreactivity of Anatase TiO2 Nanosheets with Dominant {001} Facets. *J. Am. Chem. Soc.* **2009**, *131*, 4078-4083.
(16) Siegfried, M. J.; Choi, K. S. Elucidating the effect of additives on the growth and stability of Cu2O surfaces via shape transformation of pre-grown crystals. *J. Am. Chem. Soc.* **2006**, *128*, 10356-10357.
(17) Maijenburg, A. W.; Hattori, A. N.; De Respinis, M.; McShane, C. M.; Choi, K. S.; Dam, B.; Tanaka, H.; ten Elshof, J. E. Ni and p-Cu2O Nanocubes with a Small Size Distribution by Templated Electrodeposition and Their Characterization by Photocurrent Measurement. *ACS Appl. Mater. Interfaces* **2013**, *5*, 10938-10945.
(18) Ma, L. Y.; Lee, S.; DeMuth, J.; Maldonado, S. Direct electrochemical deposition of crystalline silicon nanowires at T >= 60 degrees C. *RSC Adv.* **2016**, *6*, 78818-78825.
(19) Yanson, A. I.; Rodriguez, P.; Garcia-Araez, N.; Mom, R. V.; Tichelaar, F. D.; Koper, M. T. M. Cathodic Corrosion: A Quick, Clean, and Versatile Method for the Synthesis of Metallic Nanoparticles. *Angew. Chem. Int. Ed.* **2011**, *50*, 6346-6350.
(20) Rodriguez, P.; Tichelaar, F. D.; Koper, M. T. M.; Yanson, A. I. Cathodic Corrosion as a Facile and Effective Method To Prepare Clean Metal Alloy Nanoparticles. *J. Am. Chem. Soc.* **2011**, *133*, 17626-17629.
(21) Bennett, E.; Monzo, J.; Humphrey, J.; Plana, D.; Walker, M.; McConville, C.; Fermin, D.; Yanson, A.; Rodriguez, P. A Synthetic Route for the Effective Preparation of Metal Alloy Nanoparticles and Their Use as Active Electrocatalysts. *ACS Cat.* **2016**, *6*, 1533-1539.
(22) Rodriguez, P.; Plana, D.; Fermin, D. J.; Koper, M. T. M. New insights into the catalytic activity of gold nanoparticles for CO oxidation in electrochemical media. *J. Catal.* **2014**, *311*, 182-189.
(23) Elwakkad, S. E. S.; Rizk, H. A.; Ebaid, I. G. The Electrochemical Behavior of the Tungsten Electrode and the Nature of the Different Oxides of the Metal. *J. Phys. Chem.* **1955**, *59*, 1004-1008.
(24) Elbasiouny, M. S.; Hassan, S. A.; Hefny, M. M. On the Electrochemical-Behavior of Tungsten - The Formation and Dissolution of Tungsten-Oxide in Sulfuric-Acid-Solutions. *Corros. Sci.* **1980**, *20*, 909-917.
(25) Lu, F.; Ji, X. B.; Yang, Y. C.; Deng, W. T.; Banks, C. E. Room temperature ionic liquid assisted well-dispersed core-shell tin nanoparticles through cathodic corrosion. *RSC Adv.* **2013**, *3*, 18791-18793.
(26) Yanson, A. I.; Antonov, P. V.; Rodriguez, P.; Koper, M. T. M. Influence of the electrolyte concentration on the size and shape of platinum nanoparticles synthesized by cathodic corrosion. *Electrochim. Acta* **2013**, *112*, 913-918.
(27) Duca, M.; Rodriguez, P.; Yanson, A. I.; Koper, M. T. M. Selective Electrocatalysis on Platinum Nanoparticles with Preferential (100) Orientation Prepared by Cathodic Corrosion. *Top. Catal.* **2014**, *57*, 255-264.
(28) Seabold, J. A.; Zhu, K.; Neale, N. R. Efficient solar photoelectrolysis by nanoporous Mo: BiVO4 through controlled electron transport. *Phys. Chem. Chem. Phys.* **2014**, *16*, 1121-1131.
(29) Ng, Y. H.; Iwase, A.; Kudo, A.; Amal, R. Reducing Graphene Oxide on a Visible-Light BiVO4 Photocatalyst for an Enhanced Photoelectrochemical Water Splitting. *J. Phys. Chem. Lett.* **2010**, *1*, 2607-2612.
(30) Hersbach, T. J. P.; Mints, V. A.; Calle-Vallejo, F.; Yanson, A. I.; Koper, M. T. M. Anisotropic etching of rhodium and gold as the onset of nanoparticle formation by cathodic corrosion. *Farad. Discuss.* **2016**, *193*, 207-222.
(31) Townsend, T. K.; Sabio, E. M.; Browning, N. D.; Osterloh, F. E. Improved Niobate Nanoscroll Photocatalysts for Partial Water Splitting. *Chemsuschem* **2011**, *4*, 185-190.
(32) Seabold, J. A.; Choi, K. S. Efficient and Stable Photo-Oxidation of Water by a Bismuth Vanadate Photoanode Coupled with an Iron Oxyhydroxide Oxygen Evolution Catalyst. *J. Am. Chem. Soc.* **2012**, *134*, 2186-2192.
(33) Zhong, D. K.; Choi, S.; Gamelin, D. R. Near-Complete Suppression of Surface Recombination in Solar Photoelectrolysis by "Co-Pi" Catalyst-Modified W:BiVO4. *J. Am. Chem. Soc.* **2011**, *133*, 18370-18377.
(34) Park, H. S.; Kweon, K. E.; Ye, H.; Paek, E.; Hwang, G. S.; Bard, A. J. Factors in the Metal Doping of BiVO4 for Improved Photoelectrocatalytic Activity as Studied by Scanning Electrochemical Microscopy and First-Principles Density-Functional Calculation. *J. Phys. Chem. C* **2011**, *115*, 17870-17879.
(35) Chen, L.; Toma, F. M.; Cooper, J. K.; Lyon, A.; Lin, Y. J.; Sharp, I. D.; Ager, J. W. Mo-Doped BiVO4 Photoanodes Synthesized by Reactive Sputtering. *Chemsuschem* **2015**, *8*, 1066-1071.
(36) Feng, C. X.; Wang, S. Z.; Geng, B. Y. Ti(IV) doped WO3 nanocuboids: fabrication and enhanced visible-light-driven photocatalytic performance. *Nanoscale* **2011**, *3*, 3695-3699.

(37) Theerthagiri, J.; Senthil, R. A.; Malathi, A.; Selvi, A.; Madhavan, J.; Ashokkumar, M. Synthesis and characterization of a CuS-WO3 composite photocatalyst for enhanced visible light photocatalytic activity. *RSC Adv.* **2015**, *5*, 52718-52725.
(38) Liew, S. L.; Zhang, Z.; Goh, T. W. G.; Subramanian, G. S.; Seng, H. L. D.; Hor, T. S. A.; Luo, H. K.; Chi, D. Z. Yb-doped WO3 photocatalysts for water oxidation with visible light. *Int. J. Hydrogen Energy* **2014**, *39*, 4291-4298.
(39) Radecka, M.; Sobas, P.; Wimbicka, M.; Rekas, M. Photoelectrochemical properties of undoped and Ti-doped WO3. *Physica B-Condens. Matter* **2005**, *364*, 85-92.
(40) Martyanov, I. N.; Uma, S.; Rodrigues, S.; Klabunde, K. J. Structural defects cause TiO2-based photocatalysts to be active in visible light. *Chem. Comm.* **2004**, 2476-2477.
(41) Zhuang, J. D.; Dai, W. X.; Tian, Q. F.; Li, Z. H.; Xie, L. Y.; Wang, J. X.; Liu, P.; Shi, X. C.; Wang, D. H. Photocatalytic Degradation of RhB over TiO2 Bilayer Films: Effect of Defects and Their Location. *Langmuir* **2010**, *26*, 9686-9694.
(42) Helms, B. A.; Williams, T. E.; Buonsanti, R.; Milliron, D. J. Colloidal Nanocrystal Frameworks. *Adv. Mater.* **2015**, *27*, 5820-5829.
(43) Singh, A.; Lindquist, B. A.; Ong, G. K.; Jadrich, R. B.; Ha, H.; Ellison, C. J.; Truskett, T. M.; Milliron, D. J. Linking Semiconductor Nanocrystals into Gel Networks through All-Inorganic Bridges. *Angew. Chem. Int. Ed.* **2015**, *54*, 14840-14844.

Table of Contents/Abstract Graphic